Application of TCSC in Enhancing Dynamic Performance of Interconnected Multimachine Power System

Rudy Gianto

Department of Electrical Engineering, Tanjungpura University, Indonesia
rudygianto@gmail.com

Abstract: TCSCs (Thyristor Controlled Series Capacitors) have been used by many modern electric power system utilities for regulating power flow and increasing power transfer capability. The ability in regulating the transmittable power flow also implies the potential application of the device for the improvement of system stability and dynamic performance. The research reported in this paper investigates the application of TCSC in improving dynamic performance of large interconnected electric power system. Simulation results show that the TCSC provides better system stability and dynamic performance. The results have also been verified through eigenvalues analysis and confirmed by time-domain simulations.

Keywords: TCSC, FACTS, system stability, dynamic performance, power system.

1. Introduction

Maintaining good dynamic performance or system stability of an electric power system is necessary for secure system operation. An unstable power system will cause loss of synchronism of the interconnected synchronous generators in the system. This situation leads to a dangerous system operation where some of the generators are unable to keep running in parallel and will be separated from the system. If the remaining connected generators are not capable of meeting the load demand, large-scale interruptions of services may occur and in turn they will cause system collapse.

Traditionally, power system stability has been improved by using PSS (Power System Stabilizer). PSS has been used for many years to enhance system dynamic performance. However, the use of PSS may not be, in some cases, effective in improving system stability, particularly with increasing transmission line loading over long distances [1, 2]. In such cases, other effective alternatives are needed in addition to PSS.

Nowadays, many modern power systems have been equipped with FACTS (Flexible AC Transmission System) devices. The primary purpose of these devices is to control voltage and active- and/or reactive-power flow in the transmission system. However, by using supplementary controller, it is expected to obtain the devices secondary function of improving system stability and dynamic performance [3, 4]. This supplementary damping controller (SDC) is augmented with FACTS devices main control systems, and often referred to as FACTS device stabilizer (FDS).

TCSC is the second generation of FACTS devices. TCSC uses power electronics devices to control capacitor bank connected in series with transmission line [5]. It is equivalent to a controllable reactance inserted in series with a line to compensate the effect of the line inductance. The net transfer reactance is reduced and leads to an increase in power transfer capability. The voltage profiles are also improved due to the insertion of series capacitance in the line. The TCSC capability in controlling transmittable power also implies the potential application of the device for the enhancement of system stability and dynamic performance.

The application of TCSC in power system stability improvement has been investigated by several researchers. Recent results can be found in [6-10]. In [6-9], TCSC was used to enhance the stability of small power systems. Although, the TCSC has been successfully applied to enhance stability of small power systems, its performance, however, on larger interconnected multi-machine power systems is still unclear. In [10], an optimization algorithm-based fuzzy adaptive bacterial foraging (FAFB) has been used to design the PSS and TCSC for damping

Received: January 3rd, 2016. Accepted: December 7th, 2016
DOI: 10.15676/ijeei.2016.8.4.7

the low frequency oscillations of the power system. However, the investigation results reported in the paper were not very convincing since the eigenvalue analysis was not used to confirm the results.

A general design method or procedure has been proposed in [11-13] for optimal control coordination amongst PSSs and FACTS devices. In the method, the eigenvalue-eigenvector equations are used as a set of equality constraints in the optimization by which the controllers parameters are determined, and optimal dampings of the specified electromechanical modes are achieved. The method has been developed in the context of, and applied to small power systems. In the investigation, the effectiveness of the method in designing controllers that guarantee and improve power system dynamic performance has been confirmed.

Therefore, against the above background, the objective of the present paper is to extend the investigation to larger interconnected multi-machine electric power systems. Specifically, the main contributions of the present paper can be described as follows: (i) development of general mathematical model of multi-TCSC in multimachine power system environment for stability studies. By using the mathematical formulation proposed, any number of TCSCs (installed in any lines) can be modeled without difficulty. Also it can be applied to any size of power system; (ii) application and extension of the method for control coordination of PSSs and FACTS devices proposed in [11-13] to large multimachine power system, with a particular reference to the enhancement of interarea mode damping. The performance of FACTS device in improving system stability and dynamic performance is validated by eigenvalues analysis and time-domain simulations of the power system.

2. Power System Dynamic Model

In the context of power system stability, the system dynamic responses derive from the rotating machines (including their controllers) and FACTS devices which are interconnected by the network. On this basis, the dynamic modeling required for the study related to dynamic performance has two main aspects to be considered: the first is that of the modeling of individual components of power systems, and the second the overall system model where their interconnection is represented.

In general, the differential/algebraic equations derived from the system models are nonlinear. In preparation for the stability study, the individual power system component equations can be linearized about a specified operating point. Given the frequency range encountered in the stability study, the network which has the function of interconnecting the above items of system component will be modeled in a static form which combines the network with other items of power system in forming the overall system model.

A. Synchronous Machine Model

In this paper, the synchronous machine is represented by the fifth-order model in the d-q axes having the rotor frame of reference [14]:

$$\dot{\mathbf{\Psi}}_r = \mathbf{A}_m \mathbf{\Psi}_r + \mathbf{F}_m \mathbf{I}_S + \mathbf{V}_r \tag{1}$$

$$\dot{\omega}_r = (P_m - P_e)/M \tag{2}$$

$$\dot{\delta}_r = \omega_r - \omega_R \tag{3}$$

where Ψ_r , ω_r , and δ_r are rotor flux linkage vector, rotor angular frequency and rotor angle respectively; $\boldsymbol{V}_r = \begin{bmatrix} E_{fd} & 0 & 0 \end{bmatrix}^T$ is the rotor voltage vector; P_m and P_e are the mechanical and electrical powers respectively; M is calculated from $M = 2H/\omega_R$ (H is the machine inertia constant and ω_R is the synchronous speed); A_m and F_m are the matrices depending on machine parameters; I_S is the stator current vector, and E_{fd} is the field voltage. The transients in the rotor

fluxes set up by the field winding, and damper windings on the d and q axes are represented in the model.

Electrical power P_e in (2) can be expressed in terms of generator current as follows:

$$P_e = \mathbf{B}_m \mathbf{I}_s + \mathbf{C}_m \mathbf{\Psi}_r \tag{4}$$

where:

$$\mathbf{B}_m = \omega_r \mathbf{I}_s^T \mathbf{G}_m \,;\, \mathbf{C}_m = \omega_r \mathbf{I}_s^T \mathbf{S}_m \tag{5}$$

Given the low frequency encountered in electromechanical transients, and to be consistent with the network model in a static form, the stator flux transients are discounted. With the stator flux linkage in a non-transient form, the relationship between the stator current vector I_s and the stator voltage vector V_s can be represented by the following algebraic equation:

$$\mathbf{V}_s = \mathbf{P}_m \mathbf{\Psi}_r - \mathbf{Z}_m \mathbf{I}_s \tag{6}$$

In (5) and (6), G_m, S_m, P_m and Z_m are the matrices depending on machine parameters and rotor angular frequency.

B. Excitation and Prime Mover Model

A wide range of block diagrams for modeling various types of excitation systems and prime-mover controllers have been developed by the IEEE [15, 16]. Irrespective of the control block diagram, the first-order differential equation set for describing the excitation system dynamics can be arranged in the following form:

$$\dot{\mathbf{x}}_e = \mathbf{A}_e \mathbf{x}_e + \mathbf{C}_e |V_s| + \mathbf{B}_e V_{PSS} + \mathbf{D}_e V_s^{ref} \tag{7}$$

where $\boldsymbol{x}_e$ is the state vector for the excitation system; V_s is the synchronous machine terminal voltage; V_{PSS} is the supplementary signal from the PSS; V_s^{ref} is the voltage reference; A_e, B_e, C_e and D_e are matrices of constant values which depend on the gains and time constants of the controller.

The system dynamics of the prime-mover controller can also be represented by the set of first-order differential equation as follows:

$$\dot{\mathbf{x}}_g = \mathbf{A}_g \mathbf{x}_g + \mathbf{C}_g \omega_r + \mathbf{B}_g \omega^{ref} + \mathbf{D}_g P_m^0 \tag{8}$$

where $\boldsymbol{x}_g$ is the state vector for the prime-mover controller; ω^{ref} is the speed reference; P_m^0 is the initial power; A_g, C_g, B_g and D_g are matrices of constant values which depend on the gains and time constants of the controller.

C. PSS Model

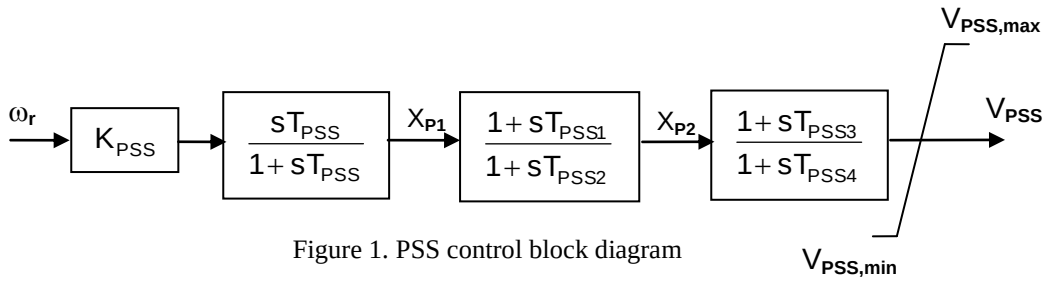

Figure 1. PSS control block diagram

Figure 1 shows the general structure of a PSS [17] which is adopted in this paper. The structure consists of a gain block, a washout, lead-lag blocks and a limiter. A washout term/filter (i.e. with a time derivative operator) in the PSS structure is needed to guarantee that

the PSS responds only to disturbances, and does not respond to any steady-state condition, when speed or power is input. Here, the rotor speed is used for the PSS input. The PSS output is added to the exciter voltage error signal and served as a supplementary signal.

The state equation derived by examining the PSS transfer functions can be arranged in the following form:

$$\dot{\mathbf{x}}_p = \mathbf{A}_p \mathbf{x}_p + \mathbf{C}_p \dot{\omega}_r \tag{9}$$

where $\boldsymbol{x}_p = \begin{bmatrix} x_{P1} & x_{P2} & V_{PSS} \end{bmatrix}^T$ is the vector of state variables of the PSS; A_p and C_p are matrices the elements of which depend on the gains and time constants of the PSS controllers.

D. TCSC and Supplementary Controller Model

In Figure 2 is shown in a block diagram form the control system of a TCSC [6, 18] used in the present work. In Figure 2, X_t is the reactance of TCSC. The TCSC control block diagram contains Proportional-Integral (PI) controller block and the block that represents the TCSC thyristor firing delays. The PI block is the TCSC main controller. The power flow control is usually implemented with a slow controller which is typical for a PI controller with a large time constant. For stability improvement purpose, a supplementary signal (X_{SDC}) derived from a separate controller is input to the main controller as shown in Figure 2. The state equations for the TCSC main control system can be arranged as follows:

$$\dot{\mathbf{x}}_t = \mathbf{A}_t \mathbf{x}_t + \mathbf{B}_t X_{SDC} + \mathbf{C}_t P_T + \mathbf{D}_t \dot{P}_T + \mathbf{E}_t P^{ref} \tag{10}$$

where $\boldsymbol{x}_t = \begin{bmatrix} x_{PF} & X_t \end{bmatrix}^T$ is the state vector for the TCSC main control system; A_t, B_t, C_t, D_t and E_t are matrices the elements of which depend on the gains and time constants of the controllers.

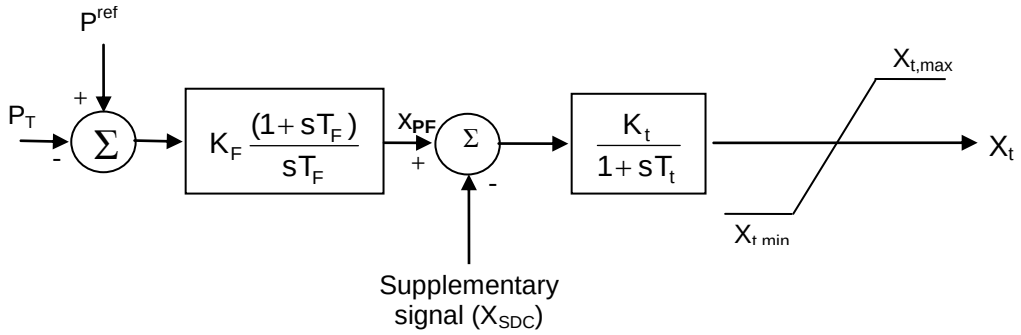

Figure 2. Control block diagram of TCSC

Dynamic performance improvement with FACTS devices is effected through power modulation by a supplementary damping controller (SDC). Figure 3 shows the control block diagram used in the present work [12, 13].

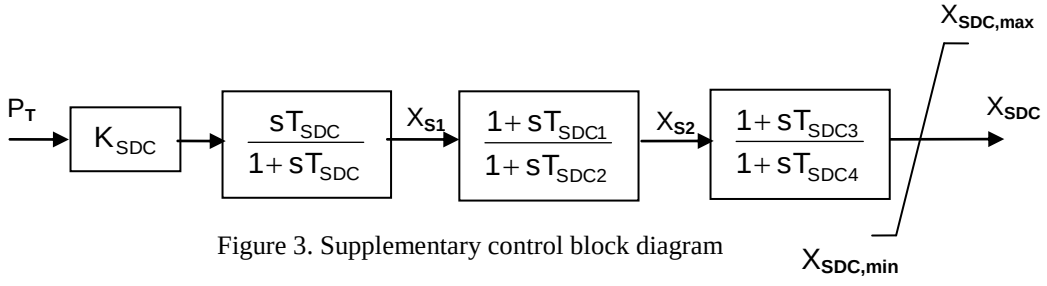

Figure 3. Supplementary control block diagram

The state equation for the supplementary controller can be written in compact form as follows:

$$\dot{\boldsymbol{x}}_{su} = \boldsymbol{A}_{su}\boldsymbol{x}_{su} + \boldsymbol{C}_{su}\dot{P}_T \tag{11}$$

where $\boldsymbol{x}_{su} = \begin{bmatrix} x_{s1} & x_{s2} & X_{SDC} \end{bmatrix}^T$ is the vector of state variables of the supplementary controller; A_{su} and C_{su} are matrices the elements of which depend on the gains and time constants of the controller.

D. Multi-Machine Power System Network Model

Figure 4 shows an NB-node power system considered in this paper. It is to be assumed that NG generators are connected to the power system. The network nodal current vector I and nodal voltage vector V for the system are related by:

$$\boldsymbol{I} = \boldsymbol{Y}\boldsymbol{V} \tag{12}$$

where Y is the system admittance matrix.

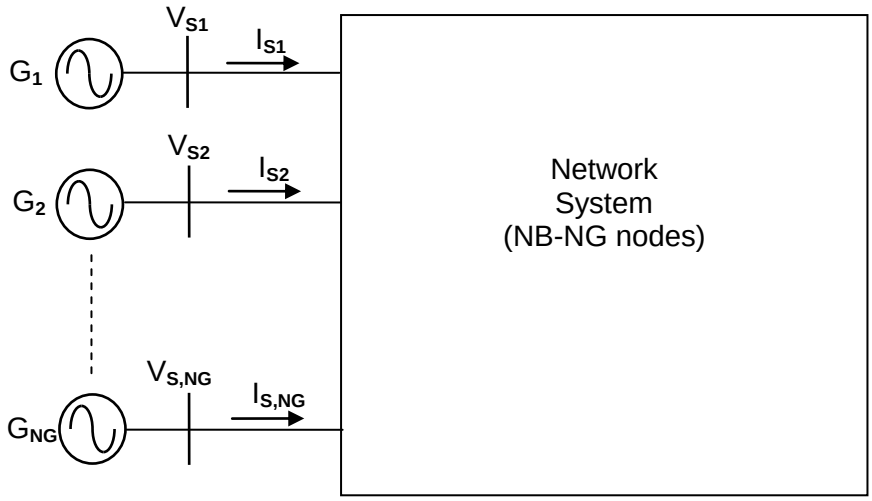

Figure 4. Multi-machine power system

All of the quantities in (12) are, in general, complex numbers. Separating (12) into real and imaginary parts and rearranging, leads to the following equation where all of the vector/matrix coefficients are real:

$$\boldsymbol{I}_N = \boldsymbol{Y}_N\boldsymbol{V}_N \tag{13}$$

where:

$$\begin{aligned} \mathbf{I}_N &= \begin{bmatrix} re(I_1) & im(I_1) & \vdots & re(I_2) & im(I_2) & \vdots & \cdots & \vdots & re(I_{NB}) & im(I_{NB}) \end{bmatrix}^T \\ \mathbf{V}_N &= \begin{bmatrix} re(V_1) & im(V_1) & \vdots & re(V_2) & im(V_2) & \vdots & \cdots & \vdots & re(V_{NB}) & im(V_{NB}) \end{bmatrix}^T \end{aligned} \tag{14}$$

and:

$$\mathbf{Y}_{\mathrm{N}} = \begin{bmatrix} re(Y_{11}) & -im(Y_{11}) & \vdots & re(Y_{12}) & -im(Y_{12}) & \vdots & \cdots & \vdots & re(Y_{1,NB}) & -im(Y_{1,NB}) \\ im(Y_{11}) & re(Y_{11}) & \vdots & im(Y_{12}) & re(Y_{12}) & \vdots & \cdots & \vdots & im(Y_{1,NB}) & re(Y_{1,NB}) \\ \cdots\cdots & \cdots\cdots & \vdots & \cdots\cdots & \cdots\cdots & \vdots & \cdots & \vdots & \cdots\cdots & \cdots\cdots \\ re(Y_{21}) & -im(Y_{21}) & \vdots & re(Y_{22}) & -im(Y_{22}) & \vdots & \cdots & \vdots & re(Y_{2,NB}) & -im(Y_{2,NB}) \\ im(Y_{21}) & re(Y_{21}) & \vdots & im(Y_{22}) & re(Y_{22}) & \vdots & \cdots & \vdots & im(Y_{2,NB}) & re(Y_{2,NB}) \\ \cdots\cdots & \cdots\cdots & \vdots & \cdots\cdots & \cdots\cdots & \vdots & \cdots & \vdots & \cdots\cdots & \cdots\cdots \\ \vdots & \vdots & \vdots & \vdots & \vdots & \vdots & \ddots & \vdots & \vdots & \vdots \\ \cdots\cdots & \cdots\cdots & \vdots & \cdots\cdots & \cdots\cdots & \vdots & \cdots & \vdots & \cdots\cdots & \cdots\cdots \\ re(Y_{NB,1}) & -im(Y_{NB,1}) & \vdots & re(Y_{NB,2}) & -im(Y_{NB,2}) & \vdots & \cdots & \vdots & re(Y_{NB,NB}) & -im(Y_{NB,NB}) \\ im(Y_{NB,1}) & re(Y_{NB,1}) & \vdots & im(Y_{NB,2}) & re(Y_{NB,2}) & \vdots & \cdots & \vdots & im(Y_{NB,NB}) & re(Y_{NB,NB}) \end{bmatrix} \tag{15}$$

In (12), the static loads of constant admittance form and fixed form of reactive power compensation are included in the system admittance matrix. In this way, the nodal currents in vector I are non-zero only at generator nodes. Therefore, (12) can be partitioned as follows:

$$\begin{bmatrix} \mathbf{I}_{SN} \\ \cdots\cdots \\ \mathbf{I}_{LN} = \mathbf{0} \end{bmatrix} = \begin{bmatrix} \mathbf{Y}_{SS} & \vdots & \mathbf{Y}_{SL} \\ \cdots\cdots & \cdots & \cdots\cdots \\ \mathbf{Y}_{LS} & \vdots & \mathbf{Y}_{LL} \end{bmatrix} \begin{bmatrix} \mathbf{V}_{SN} \\ \cdots\cdots \\ \mathbf{V}_{LN} \end{bmatrix} \tag{16}$$

where:
S: set of generator nodes
L: set of non-generator nodes
I_{SN}, V_{SN}: vectors of network nodal currents and voltages at generator nodes respectively
V_{LN}: vector of nodal voltages at the remaining nodes in the system
Y_{SS}, Y_{SL}, Y_{LS} and Y_{LL}: submatrices from partitioning of Y matrix

Based on (16), the following equations are obtained:

$$\mathbf{I}_{SN} = \mathbf{Y}_{SS}\mathbf{V}_{SN} + \mathbf{Y}_{SL}\mathbf{V}_{LN} \tag{17}$$

$$\mathbf{0} = \mathbf{Y}_{LS}\mathbf{V}_{SN} + \mathbf{Y}_{LL}\mathbf{V}_{LN} \tag{18}$$

The nodal voltage vector V_{SN} and nodal current vector I_{SN} in (17) and (18) are in the network D-Q frame of reference. By transforming the variables V_{SN} and I_{SN} into their corresponding d-q components (V_{sM} and I_{sM}) using frame of reference transformation, (17) and (18) become:

$$\mathbf{T}_{\delta M}\mathbf{I}_{sM} = \mathbf{Y}_{SS}\mathbf{T}_{\delta M}\mathbf{V}_{sM} + \mathbf{Y}_{SL}\mathbf{V}_{LN} \tag{19}$$

$$\mathbf{0} = \mathbf{Y}_{LS}\mathbf{T}_{\delta M}\mathbf{V}_{sM} + \mathbf{Y}_{LL}\mathbf{V}_{LN} \tag{20}$$

where:

$$\mathbf{T}_{\delta M} = diag\left(\mathbf{T}_{\delta 1}, \mathbf{T}_{\delta 2}, \cdots, \mathbf{T}_{\delta, NG}\right) \tag{21}$$

It can be seen from the discussion that the network model for multi-machine power system is described by two sets of algebraic equations (19) and (20). It is also to be noted that the algebraic (non-state) variables of the network model of the system are V_{sM}, I_{sM} and V_{LN}.

E. Model of Multi-Machine Power System with TCSCs

Figure 5 shows a multi-machine power system installed with TCSCs. In order to illustrate the mathematical formulation for modeling the power system network, it is to be assumed that the TCSCs are installed as shown in Figure 5. In Figure 5, NT is the number of TCSCs.

In D-Q frame of reference and partitioned form, the network model for the multi-machine power system installed with TCSCs can be described by:

$$\begin{bmatrix} \mathbf{I}_{SN} \\ \cdots\cdots \\ \mathbf{I}_{LN} = \mathbf{0} \end{bmatrix} = \begin{bmatrix} \mathbf{Y}_{SS} & \vdots & \mathbf{Y}_{SL} \\ \cdots\cdots & \cdots & \cdots\cdots \\ \mathbf{Y}_{LS} & \vdots & \mathbf{Y}_{LL} + \mathbf{Y}_{FT} \end{bmatrix} \begin{bmatrix} \mathbf{V}_{SN} \\ \cdots\cdots \\ \mathbf{V}_{LN} \end{bmatrix} \tag{22}$$

The submatrix Y_{FT} in (22) has the same dimension as submatrix Y_{LL} and is given by:

$$\mathbf{Y}_{FT} = \begin{array}{c} \\ \end{array}
\begin{array}{c|c|cc|cc|cc|cc|c|c}
 & & \multicolumn{2}{c|}{L_{x1}} & \multicolumn{2}{c|}{L_{x2}} & \multicolumn{2}{c|}{L_{v1}} & \multicolumn{2}{c|}{L_{v2}} & & \\
L_{NG+} & \cdots & & & & & & & & & \cdots & L_{NB} \\
\hline
\cdots & \cdots & \cdots & \cdots & \cdots & \cdots & \cdots & \cdots & \cdots & \cdots & \cdots & \cdots \quad L_{NG+1} \\
\vdots & & & & & & & & & & & \vdots \\
 & & & -Y_{t1} & & & & Y_{t1} & & & & \\
 & & Y_{t1} & & & & -Y_{t1} & & & & & \quad L_{x1} \\
 & & & & & -Y_{t2} & & & & Y_{t2} & & \\
 & & & & Y_{t2} & & & & -Y_{t2} & & & \quad L_{x2} \\
 & & & Y_{t1} & & & & -Y_{t1} & & & & \\
 & & -Y_{t1} & & & & Y_{t1} & & & & & \quad L_{v1} \\
 & & & & & Y_{t2} & & & & -Y_{t2} & & \\
 & & & & -Y_{t2} & & & & Y_{t2} & & & \quad L_{v2} \\
\vdots & & & & & & & & & & & \vdots \\
\cdots & \cdots & \cdots & \cdots & \cdots & \cdots & \cdots & \cdots & \cdots & \cdots & \cdots & \cdots \quad L_{NB}
\end{array} \tag{23}$$

Based on (22), the following equation is obtained:

$$\mathbf{0} = \mathbf{Y}_{LS}\mathbf{V}_{SN} + \left(\mathbf{Y}_{LL} + \mathbf{Y}_{FS}\right)\mathbf{V}_{LN} \tag{24}$$

Transforming the variable V_{SN} in (24) into V_{sM} leads to:

$$\mathbf{0} = \mathbf{Y}_{LS}\mathbf{T}_{\delta M}\mathbf{V}_{sM} + \left(\mathbf{Y}_{LL} + \mathbf{Y}_{FS}\right)\mathbf{V}_{LN} \tag{25}$$

The above discussion shows that the network model for multi-machine power system installed with TCSCs can be described by two sets of algebraic equations (18) and (25). It is also to be noted that the algebraic (non-state) variables of the network model of the system are V_{sM}, I_{sM} and V_{LN}.

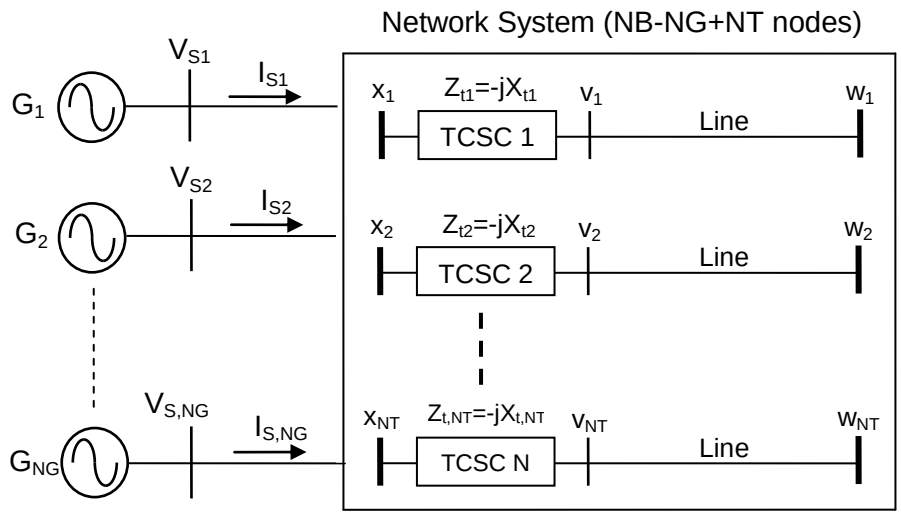

Figure 5. Multi-machine power system with TCSCs

F. System State Matrix

Previous sections show that the dynamic model of the power system installed with TCSC is described by a set of differential-algebraic equations (DAEs) which can be written in a more compact form as the following:

$$\begin{aligned} \dot{\mathbf{x}} &= \mathbf{f}(\mathbf{x},\mathbf{w}) \\ \mathbf{0} &= \mathbf{g}(\mathbf{x},\mathbf{w}) \end{aligned} \tag{26}$$

where: x is the vector of state variables; w is the vector of non-state (algebraic) variables; f and g are nonlinear vector functions the individual expressions of which have been given in the previous sections.

The small-disturbance stability model of the power system installed with TCSC is obtained by linearising the differential-algebraic equations which can also be written in a more compact form as follows:

$$\begin{pmatrix} \Delta\dot{\mathbf{x}} \\ \mathbf{0} \end{pmatrix} = \begin{pmatrix} \mathbf{J}_1 & \mathbf{J}_2 \\ \mathbf{J}_3 & \mathbf{J}_4 \end{pmatrix} \begin{pmatrix} \Delta\mathbf{x} \\ \Delta\mathbf{w} \end{pmatrix} \tag{27}$$

where J_1, J_2 , J_3 , and J_4 are matrices the elements of which are defined based on the power system initial operating condition and the parameters of the system together with its controllers. By reducing (27), the following equation is obtained:

$$\Delta\dot{\mathbf{x}} = \mathbf{A}\Delta\mathbf{x} \tag{28}$$

where $\mathbf{A} = \mathbf{J}_1 - \mathbf{J}_2\mathbf{J}_4^{-1}\mathbf{J}_3$ is the system state matrix. Eigenvalues of this matrix are needed for evaluation the stability and dynamic characteristic of the power system, and for the damping controllers design. The state matrix is the function of controllers (PSSs and TCSC devices together with their supplementary controllers) parameters.

3. Results of Investigation

A. Test System

The system in the study is based on the 10-machine 38-node power system of Figure 6 [19]. Initial investigation, where the damping controllers (PSS and/or SDC of TCSC) are not included in the system, has been carried out to determine the system oscillation damping without the controllers. Modal analysis used in the investigation shows that there are nine electromechanical modes of oscillations (inter-area and local modes). As there is a strong connection between inter-area mode of oscillations and system dynamic performance, the inter-area modes, especially the mode with the lowest damping, will be the focus of the investigation. In Table 1 are given the electromechanical inter-area mode eigenvalue, frequency, and damping ratio for the system of Figure 6. As can be seen from Table 1, the damping ratio of the inter-area mode is low which indicates poor system dynamic performance and stability. Stabilization measure is, then, required for improving the damping of the inter-area oscillation.

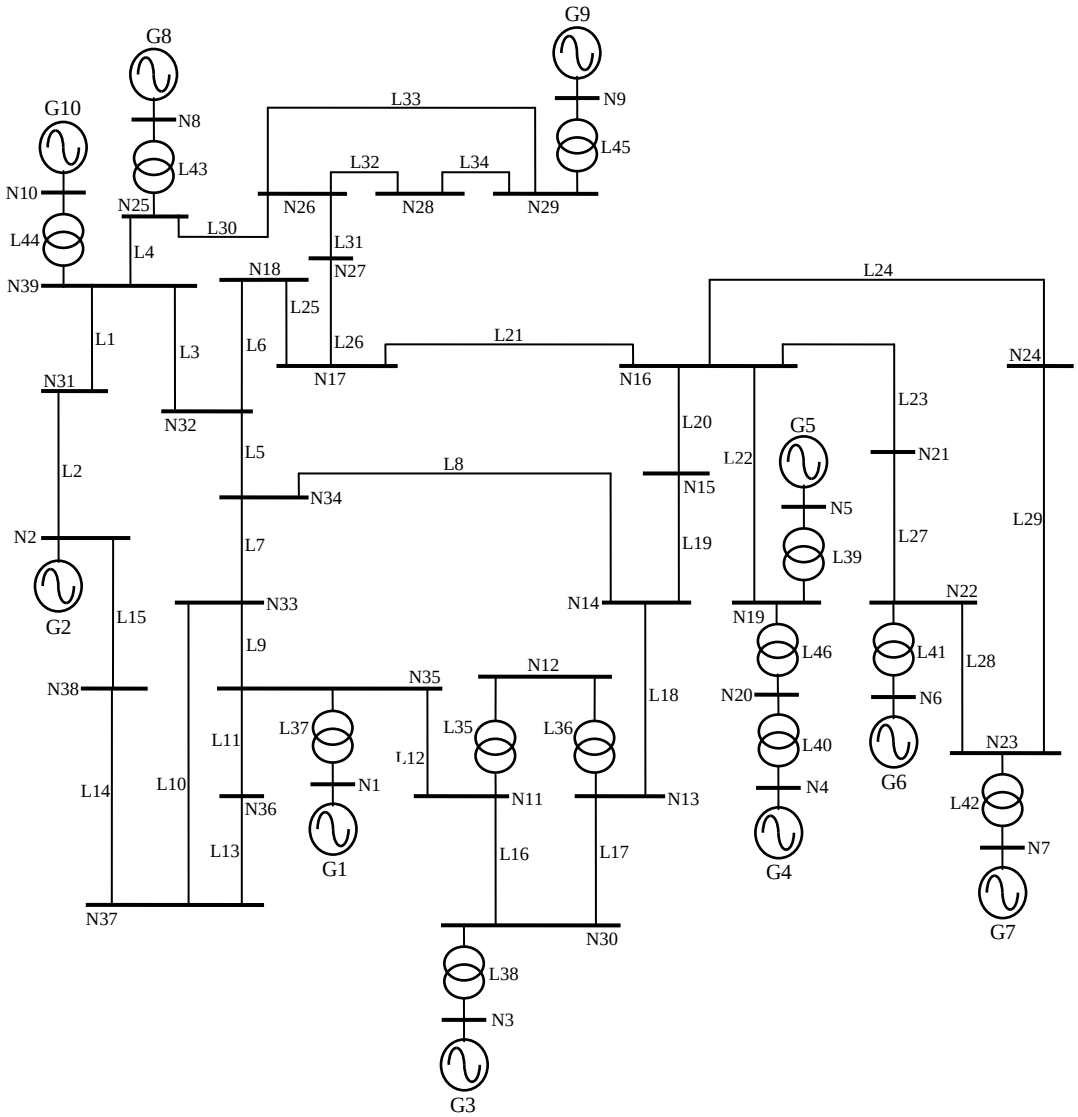

Figure 6. 10-machine 38-node power system

Therefore, in order to improve the stability, it is proposed to install two PSSs in the system (in generators G2 and G5). The locations of the PSSs have been determined using participation factor technique. In Table 2 are given the electromechanical inter-area mode eigenvalue, frequency, and damping ratio for the system with PSSs. It is to be noted that optimal values of PSSs parameters were used in the investigation. These values are given in Table 3 and were obtained using the method proposed in [11-13].

Table 1. Electromechanical inter-area mode

EIGENVALUE	FREQUENCY (HZ)	DAMPING RATIO
-0.3589 ± J4.5167	0.72	0.0792

Table 2. Electromechanical inter-area mode (system with PSSs)

EIGENVALUE	FREQUENCY (HZ)	DAMPING RATIO
-0.5937±J4.5903	0.73	0.1283

Table 3. PSSs parameters

Parameter	PSS at G2	PSS at G5
K_{PSS}	10.6312 pu	19.9858 pu
T_{PSS}	1.0016 s	1.0000 s
T_{PSS1}	0.2498 s	0.2025 s
T_{PSS2}	0.0150 s	0.0958 s
T_{PSS3}	0.1729 s	0.0547 s
T_{PSS4}	0.1396 s	0.1978 s

It can be seen from Table 2 that damping ratio of the inter-area mode increases from 0.0792 to 0.1283 with the installation of PSSs. Although it has been considered in [1, 20] that the damping ratio greater than 0.1 is acceptable; however, as mentioned in [21, 22], a minimum damping ratio of 0.15 is desirable for ensuring faster settling time of the oscillations.

B. SDC of TCSC Application

To ensure faster settling time, it is proposed to further improve system dynamic performance by installing an SDC in the TCSC in line L14. It is to be noted that the TCSC has already been installed in the system for the primary purpose of power transfer capacity improvement of the line. An opportunity is then taken to equip the TCSC installed with an SDC to provide a secondary function for damping enhancement of the electromechanical modes, particularly the inter-area mode.

In Table 4 are given the electromechanical inter-area mode eigenvalue, frequency, and damping ratio for the system where the SDC installed in the system. It is to be noted that optimal values of PSSs, TCSC, and SDC parameters were used in the investigation. These values are given in Table 5, and were also obtained using the method proposed in [11-13]. There is a damping improvement for the inter-area mode when the SDC of TCSC is installed (compare the damping ratio in Table 2 with Table 4). This results show that the TCSC and its SDC provides better system stability.

C. Time-Domain Simulations

Although the results given in Section 3.2 have been confirmed by eigenvalue calculations, it is desirable to investigate the performance of the controllers in the time-domain under a large disturbance. The disturbance is a three-phase fault on a busbar section connected to node N34 via a bus coupler. The fault is initiated at time t = 0.10 second, and the fault clearing time is 0.05 second with the bus coupler tripping.

The improvement in performance is quantified by comparing the time-domain responses in Figures 7 - 9. As the focus of the investigation is the inter-area mode, the responses used in the comparisons are those of relative speed transients between generators G2 and G5.

From the responses, it can be seen that, without controllers (PSSs and/or SDC of TCSC), the system oscillation is poorly damped and takes a considerable time to reach a stable condition (see Figure 7). Note that this result is in agreement with the eigenvalue result where the damping ratio of the oscillation is quite low and only 0.0792 (see Table 1).

Figure 8 shows the system transient with two PSSs installed in the system. There are some improvements in oscillation settling time with PSSs installed in the system (compare Figure 7 with Figure 8). This result is also in agreement with the eigenvalue result (see Table 2), where with the PSSs installed the damping ratio of the oscillation is higher (0.1283).

Further improvement in the inter-area oscillation settling time is obtained with the SDC of TCSC installed in the system. The oscillation is damped more quickly as shown in Figure 9. Figure 9 confirms a good system oscillation damping and dynamic performance when SDC is installed in the power system. This result is also in agreement with the eigenvalue result (see Table 4), where the damping ratio of the oscillation is at the highest (0.2092).

In Figure 10 is also shown in a graphical form the output of supplementary controller of TCSC during the transient period following the disturbance. The settling time of the oscillation is similar to that of Fig.9. This result is to be expected, and shows further the confirmation of the TCSC performance under large disturbance. It can be seen from Figure 10 that during a first few seconds of the transient period, the supplementary controller gives higher outputs, and therefore, provides significant contribution to the system damping and stability.

Table 4. Electromechanical inter-area mode (system with PSSs, SDC and TCSC)

EIGENVALUE	FREQUENCY (HZ)	DAMPING RATIO
-0.9975±J4.8806	0.78	0.2002

Table 5. PSSs, SDC and TCSC parameters

Controller	Parameter	Value
PSS (G2/G5)	K_{PSS}	19.9833/10.3938
	T_{PSS}	1.0000/1.0000
	T_{PSS1}	0.2851/0.2092
	T_{PSS2}	0.0459/0.0876
	T_{PSS3}	0.2182/0.0625
	T_{PSS4}	0.1061/0.1910
TCSC	K_F	0.0452 pu
	T_F	1.0009 s
	K_t	0.0732 pu
	T_t	0.0268 s
SDC	K_{SDC}	1.0011 pu
	T_{SDC}	1.0000 s
	T_{SDC1}	0.1968 s
	T_{SDC2}	0.1590 s
	T_{SDC3}	0.0255 s
	T_{SDC4}	0.1796 s

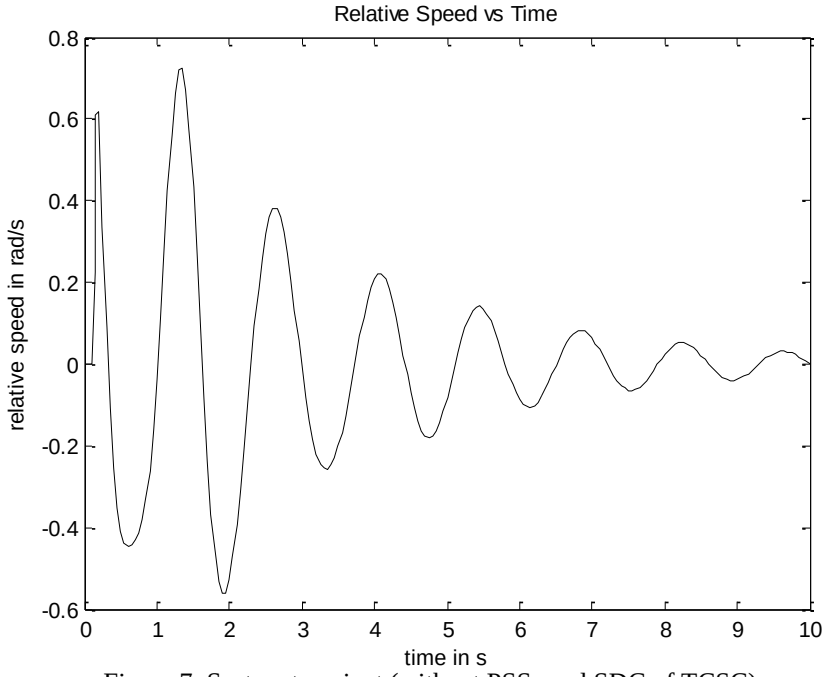

Figure 7. System transient (without PSSs and SDC of TCSC)

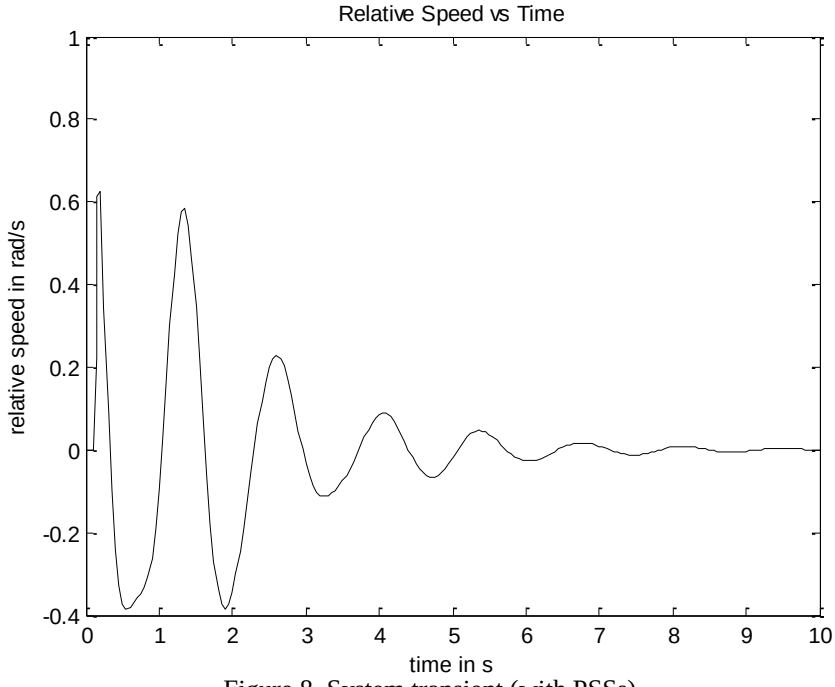

Figure 8. System transient (with PSSs)

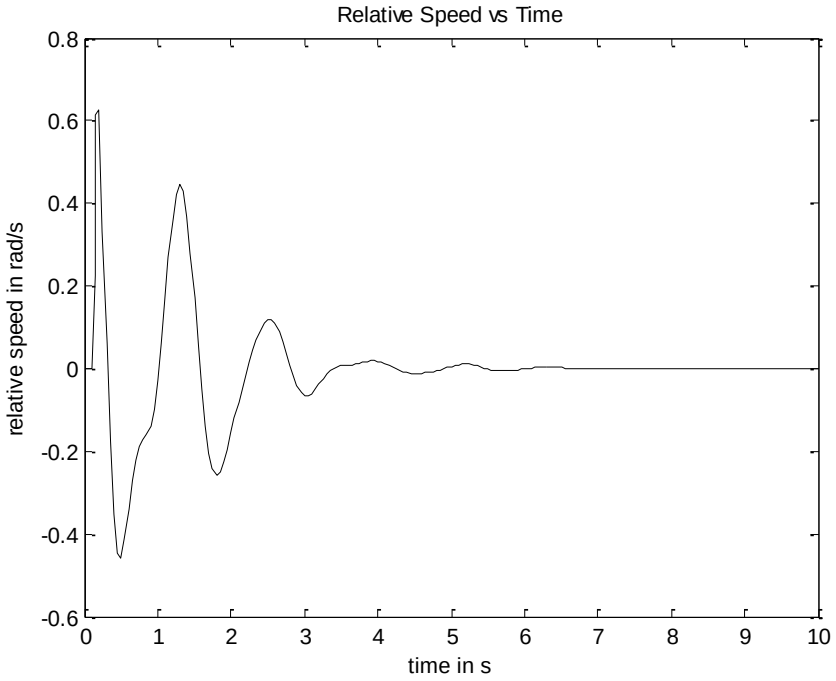

Figure 9. System transient (with PSSs and SDC of TCSC)

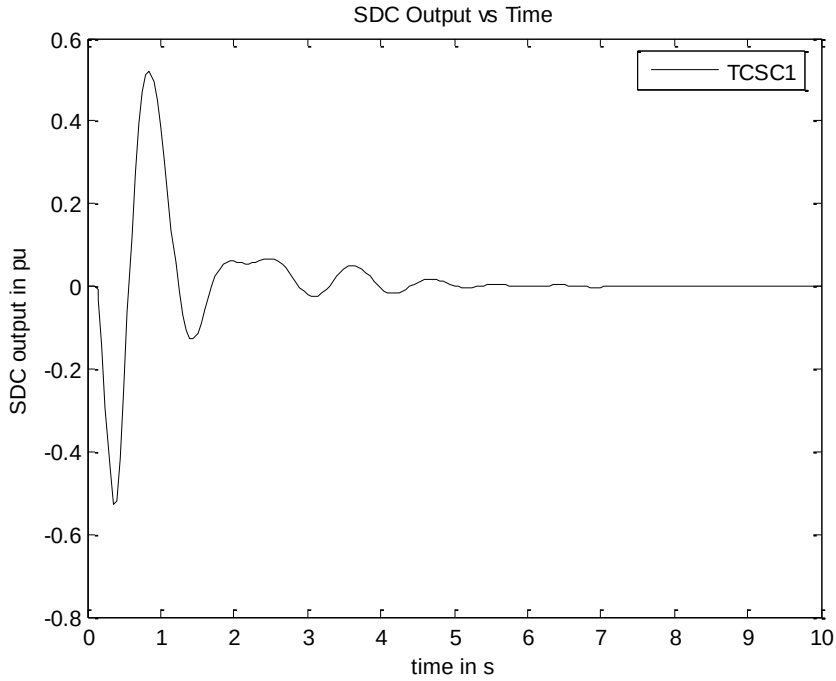

Figure 10. Transient of TCSC's supplementary controller output

4. Conclusions

In this paper, the application of TCSC and its SDC in enhancing the system oscillation damping and dynamic performance of an electric power system has been investigated. It is found that the system oscillation damping can be improved by the TCSC. This result shows

that the TCSC provides better system dynamic performance and stability of a large interconnected multi-machine power system. The result has also been verified through both eigenvalue calculations and time-domain simulations.

5. Acknowledment

The author would like to express special appreciation to the Ministry of Research, Technology and Higher Education of Indonesia (KEMENRISTEK DIKTI INDONESIA) for funding the research reported in this paper.

6. References

[1]. Cai, L.J., and Erlich, I.: 'Simultaneous coordinated tuning of PSS and FACTS damping controllers in large power systems', *IEEE Trans. Power Systems*, 2005, 20, (1), pp. 294-300.

[2]. Noroozian, M, Ghandhari, M., Andersson, G., Gronquist, J., and Hiskens, I.A.: 'A robust control strategy for shunt and series reactive compensators to damp electromechanical oscillations', *IEEE Trans. Power Delivery*, 2001, 16, (4), pp. 812-817.

[3]. Hingorani, N.G., and Gyugyi, L.: 'Understanding FACTS: concept and technology', *IEEE Press*, New York, 2000.

[4]. Hingorani, N.G.: 'Flexible AC transmission system', *IEEE Spectrum*, 1993, 30, (4), pp. 40-45.

[5]. S. Manoj and Puttaswamy P.S.: 'Importance of FACTS controllers in power systems', *International Journal of Advanced Engineering Technology*, 2011, 2, (3), pp. 207-212.

[6]. Eslami, M., Shareef, H., Mohamed, A., and Khajehzadeh, M.: 'PSS and TCSC damping controller coordinated design using GSA', Elsevier Procedia, 2012, 14, pp. 763-769.

[7]. Narrne, R., and Panda, P.C.: 'Coordinated design of PSS with Multiple FACTS controller using advanced adaptive PSO', *International Journal on Electrical Engineering and Informatics (IJEEI)*, September 2013, 5, (3), pp. 361-376.

[8]. Davarani, R.Z., and Ghazi, R.: 'Optimal simultaneous coordination of PSS and TCSC using multi objective genetic algorithm', *Journal of Electrical System (JES)*, 2013, 9, (4), pp. 410-421.

[9]. Welhazi, Y., Guesmi, T., Jaoued, I.B., and Abdallah, H.H. 'Power system stability enhancement using FACTS controllers in multimachine power systems', *Journal of Electrical System (JES)*, 2014, 10, (3), pp. 276-291.

[10]. Khorram, B., and Lesani, H.: 'Coordinated control of FACTS devices and PSS for improve the power system stability using fuzzy adaptive bacterial foraging', *International Journal on Electrical Engineering and Informatics (IJEEI)*, June 2015, 7, (2), pp. 334-351.

[11]. Nguyen, T.T., and Gianto, R.: 'Stability improvement of electromechanical oscillations by control co-ordination of PSSs and FACTS devices in multi-machine systems', *Proceedings of the IEEE PES GM 2007*, June 2007, pp. 1-7.

[12]. Nguyen, T.T., and Gianto, R.: 'Application of optimization method for control co-ordination of PSSs and FACTS devices to enhance small-disturbance stability', *Proceedings of the IEEE PES 2005/2006 Transmission and Distribution Conference & Exposition*, May 2006, pp. 1478-1485.

[13]. Nguyen, T.T., and Gianto, R.: 'Optimisation-based control co-ordination of PSSs and FACTS devices for optimal oscillations damping in multimachine power system', *IET Gener. Transm. Distrib*., 2007, 1, (4), pp.564-573.

[14]. Humpage, W.D., Bayne, J.P., and Durrani, K.E.: 'Multinode-power-system dynamic analyses', *Proc. IEE*, 1972, 119, (8), pp. 1167-1175.

[15]. IEEE Std 421.5-2005: 'IEEE recommended practice for excitation system models for power system stability studies', 2005.

[16]. IEEE Working Group: 'Dynamic models for fossil fueled steam units in power system studies', *IEEE Trans. Power Systems*, 1991, 6, (2), pp. 753-761.

[17]. Mithulananthan, N., Canizares, C.A., Reeve, J., and Rogers G.J.: 'Comparison of PSS, SVC, and STATCOM controllers for damping power system oscillations', *IEEE Trans. Power System*, 2003, 16, (2), pp. 786-792.
[18]. CIGRE TF 38.01.08: 'Modeling of power electronics equipment (FACTS) in load flow and stability programs: a representation guide for power system planning and analysis', 1999.
[19]. Pai, M.A.: 'Energy function analysis for power system stability' (Kluwer Academic Publishers, Boston, 1989).
[20]. Pourbeik, P., and Gibbard, M.J.: 'Simultaneous coordination of power system stabilizers and FACTS device stabilizers in a multimachine power system for enhancing dynamic performance', *IEEE Trans. Power Systems*, 1998, 13, (2), pp. 473-479.
[21]. Pal, B.C., Coonick, A.H., Jaimoukha, I.M., and El-Zobaidi, H.: 'A linear matrix inequality approach to robust damping control design in power systems with superconducting magnetic energy storage device', *IEEE Trans. Power Systems*, 2000, 15, (1), pp. 356-362.
[22]. Majumder, R., Chaudhuri, B., El-Zobaidi, H., Pal, B.C., and Jaimoukha, I.M.: 'LMI approach to normalised H_∞ loop-shaping design of power system damping controllers', *IEE Proc.-Gener. Transm. Distrib*., 2005, 152, (6), pp. 952-960.

Rudy Gianto received BE, ME and PhD degrees from Tanjungpura University in 1991, Bandung Institute of Technology in 1995, and The University of Western Australia in 2009 respectively. Currently, he is a Senior Lecturer at Tanjungpura University, Indonesia. He has published several international journal and conference papers. His research interests include power system stability and control, and simulation of power system dynamics.